Journal of Solid State Chemistry 184 (2011) 89–96

Contents lists available at ScienceDirect

Journal of Solid State Chemistry

journal homepage: www.elsevier.com/locate/jssc

Cation distribution and particle size effect on Raman spectrum of $CoFe_2O_4$

P. Chandramohan, M.P. Srinivasan, S. Velmurugan, S.V. Narasimhan *

Water and Steam Chemistry Division, BARCF, Kalpakkam, Tamilnadu 603102, India

ARTICLE INFO

Article history:
Received 14 May 2010
Received in revised form
6 October 2010
Accepted 16 October 2010
Available online 3 November 2010

Keywords:
Ferrites
Cation distribution
Spinel
Raman spectroscopy
Mössbauer spectroscopy and nano-materials

ABSTRACT

Mössbauer and Raman spectroscopic studies were carried out on $CoFe_2O_4$ particles synthesized with size ranging from 6 to 500 nm (bulk). Cation distribution studies were carried out on the high temperature and room temperature phases of the microcrystalline $CoFe_2O_4$ by Mössbauer and Raman spectroscopic methods. The high temperature phase of $CoFe_2O_4$ showed a decreased inversion parameter of 0.69 as compared to the value of the room temperature phase of 0.95, indicating that the structure gradually transforms towards a normal spinel. Corresponding Raman spectra for these two phases of $CoFe_2O_4$ showed a change in relative peak intensity of the vibrational mode at 695 cm^{-1}($A_{1g}(1)$) to 624 cm^{-1} ($A_{1g}(2)$). The relative peak intensity ratio, I_ν between the $A_{1g}(1)$ and $A_{1g}(2)$ vibrational mode was decreasing with lowering of inversion parameter of the $CoFe_2O_4$ spinel system. A variation of laser power on the sample surface was reflected in the cation distribution in ferrite phase. Superparamagnetic, single domain $CoFe_2O_4$ particles (6 nm) showed a 20 cm^{-1} red shift and broadening of phonon modes when compared to the macro-crystalline $CoFe_2O_4$ (500 nm). Variation of Raman shift with particle size was studied by considering the bond polarization model. Raman spectroscopic studies clearly indicate the variation in the cation distribution in nano-sized particles and distribution tending to a normal spinel structural configuration.

1. Introduction

The cation distribution in partially inverse spinels such as $CoFe_2O_4$, $MgFe_2O_4$ and $MnFe_2O_4$ is sensitive to the temperature of processing and the method adopted to synthesize these ferrites. These ferrites, having the general molecular formula MFe_2O_4 where M is divalent ion like Co, Ni, Mg and Zn, crystallize in the $Fd\bar{3}m$ space group and are useful for industry and as well in basic research due to their magnetic and electrical properties. The cation distribution in ferrites is a function of parameters such as radii of cation [1], thermal history [2–4] and particle size [5–8]. Spinels in nano-scale domain have great use because of the tunable properties with size and thermal treatment [9]. Properties have potential use in understanding the cation distribution effect in metal ion passivation studies in coolant circuits [10], catalysis, magnetically guided drug or radioactive nuclide delivery and remote detoxification [11].

Ferrites are [2,3] spinel oxides with chemical composition of $(M_{1-\delta}Fe_\delta)_{td}$ $[M_\delta Fe_{2-\delta}]_{oh}O_4$, where $\delta(0 \le \delta \le 1)$ is the inversion parameter describing the cation distribution in ferrite system. Cation distribution in spinels and its effect on the Raman spectra have been well documented in the literature [12,13]. Due to the exchange of cations between tetrahedral and octahedral sites, the Raman spectra of certain spinels get complicated [14]. In order to completely understand the ferrite system one need to have information regarding sample treatment history. Studies on nickel and magnesium aluminates have pointed out the use of Raman spectroscopy and showed the sensitivity of this technique in understanding the nature of the cation disorder due to the thermal treatment of the samples [15,16]. In the present study, we have focused on understanding cation distribution due to temperature effect and particle size. Variation of the peak position and its FWHM of Raman spectrum in $CoFe_2O_4$ with particle size was studied.

2. Experiment

2.1. Ferrite preparation

Ferrites used for the present investigation were prepared by three routes viz., double microemulsion method (DME), polymer combustion method (PC) and solid state method (SS), which are described below.

2.1.1. Solid state method

Microcrystalline $CoFe_2O_4$ was prepared by taking mixture of Co(II)CO_3 and α-Fe_2O_3 (E-Merck) in stoichiometric amounts with heat treating at 1000 °C for 36 h with intermittent mixing. After heat treatment of the sample at 1000 °C, samples were cooled by two different methods: (i) controlled cooling at a rate of 3.5 °C/min

* Corresponding author.
E-mail addresses: svn.1948@gmail.com, svn@igcar.gov.in (S.V. Narasimhan).

0022-4596/$ - see front matter © 2010 Elsevier Inc. All rights reserved.
doi:10.1016/j.jssc.2010.10.019

to ambient temperature, SS(RT) (27 °C) and (ii) quenching the hot sample to (a) liquid nitrogen temperature SS(HT_N), (b) ice water temperature SS(HT_w), (c) ambient temperature SS(HT).

2.1.2. Polymer combustion method

Stoichiometric amounts of iron and cobalt [($Fe(NO_3)_3 \cdot 9H_2O$ and $Co(NO_3)_2 \cdot 4H_2O$ (E-Merck)] in the form of metal nitrate solution were added to the 10% aqueous solution of poly vinyl alcohol. Metal ion to monomer ratio of 1:10 was maintained for syntheses. The mixture containing metal ions and polymer was allowed to form a gel and dried at 80–90 °C for 24 h time duration. One sample of the dried mass was fired in muffle furnace at 500 °C for 3 h to form the spinel oxide (PC-500). Two other samples of the dried gel were heat treated at 700 °C (PC-700) and 900 °C (PC-900), respectively.

2.1.3. Double microemulsion method

Microemulsions were prepared by using toluene as organic phase, sodium dodecylsulfate (SDS) and 1-pentanol as surfactant and co-surfactant. Stoichiometric metal nitrate salts (($Fe(NO_3)_3 \cdot 9H_2O$ and $Co(NO_3)_2 \cdot 4H_2O$) with total metal ion concentration of 3 mmole were taken in the aqueous phase. Water to surfactant ratio (W) of 5 was maintained for the preparation of microemulsions. Microemulsions were prepared by the titration method. The mixture of toluene, SDS and water with metal salts was titrated using 1-pentanol. End point or microemulsion phase is indicated by clear solution formation. Metal ion precipitation was carried out by taking alkali microemulsion using 5.5 mmole of sodium hydroxide (NaOH) in aqueous phase. Precipitated metal hydroxides were centrifuged and washed repeatedly with 18 MΩ water, followed by dry acetone and then the precipitate thus collected was dried at 100 °C. Finally, the precipitate was heat treated at 500 °C for 3 h to get the oxide (DME).

2.2. Characterization

Mössbauer spectra were recorded on samples with a 25 mCi ^{57}Co source in rhodium matrix at room temperature. Spectrometer was operated in constant acceleration mode. Velocity transducer (Wissel, Germany) was calibrated using α-Fe. Fitting of data was carried out with NORMOS least-squares fitting software and using Lorenzian shape function. The isomer shift value of the samples are reported against α-Fe at room temperature. Raman spectra were recorded on the sample using HORIBA Jobin Yvon HR 800 spectrometer with 514.5 nm Ar^+ ion laser. Laser power was optimized to 0.5 mW on the sample surface after taking into consideration the (S/N) ratio and sample degradation. Raman spectra acquisition was carried out for 60 s using a 100 × objective lens and 1800 gr/mm grating. Surface area measurements were carried out using B.E.T surface area analyzer (Sorptomatic 1990) with N_2 gas adsorption. X-ray diffraction studies were carried out on all the samples using Cu$K\alpha$ line with Philips spectrometer. Morphology and crystallinity of nano-particles were obtained by transmission electron microscopy (TEM) using JEM 3010 equipment from JEOL. LaB_6 filament and electron beam energy of 200 keV was used for collecting the images. Selected area electron diffraction (SAED) pattern was taken on the selected particle.

3. Result and discussion

3.1. Characterization for phase and size

The (2,3) ferrites, MFe_2O_4 structure consists of a cubic close packed (CCP) array of anion with 64 tetrahedral voids and 32 octahedral voids where one eighth of tetrahedral voids and half of octahedral voids are occupied by cations. In normal spinels, divalent and trivalent ions occupy tetrahedral and octahedral sites, respectively. Complete replacement of divalent ion in tetrahedral site by trivalent ion results in an inverse spinel structure, for which the extent of redistribution is given by inversion parameter δ ($0 \le \delta \le 1$), $(M_{1-\delta}Fe_\delta)_{td}[M_\delta Fe_{2-\delta}]_{oh}O_4$.

Fig. 1(a–c) shows the XRD patterns of $CoFe_2O_4$ prepared by DME, PC and SS routes. Reflections correspond to cubic structure of spinel system with following planes (220), (311), (222), (400), (422), (511) and (440) showing single phase nature of the ferrite prepared by the three respective routes. Table 1 shows the surface area and its spherical diameter of the particle prepared by DME, PC and SS routes. The ferrite synthesized by DME route showed an average size of 6 nm, the primary factor for controlling the size of the particle is hydrodynamic droplet size of the microemulsion which in turn is controlled by the water to surfactant ratio. The diameter of droplet (D) in nano-meter can be related to water/surfactant ratio (W) by $(D/2)=0.15W$ for sodium dioctyl sulfosuccinate (AOT) surfactant[17], which acts as a reaction chamber. However, it was observed that by recovering the precipitated hydroxide from the droplet and subsequent heat treatment showed an increase of the particle size compared to calculated value from the above equation. Fig. 2 shows a TEM micrograph of $CoFe_2O_4$, prepared by the microemulsion route. TEM studies detailed the narrow size distribution with spherical nature of particle. High resolution TEM image of the particles shows the crystallinity of the particle with particle size of 6.8 nm. Selected area electron diffraction (SAED) pattern also reflected the crystallinity of the ferrite particle formed with bright rings corresponding to (220), (311), (222), (400), (422),

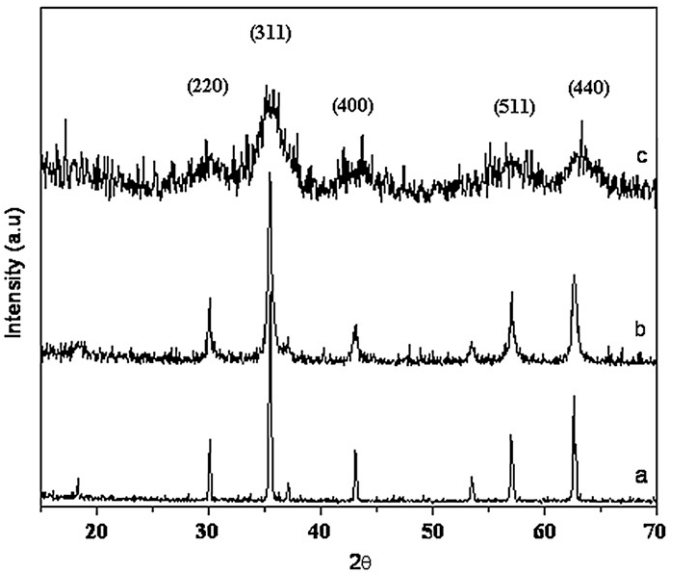

Fig. 1. XRD of $CoFe_2O_4$ prepared by (a) SS(RT) route, (b) PC-500 route and (c) DME route.

Table 1
Surface area measurements and spherical diameter of ferrite particles.

$CoFe_2O_4$	Surface area (m^2/g)	Spherical diameter (nm)
DME	188.0	6.0
PC-500	47.3	23.9
PC-700	40.5	28.0
PC-900	9.2	123.0
SS(RT)	2.4	471.6

(511) and (440) planes of spinel system. Surface area measurements on cobalt ferrite synthesized by polymer combustion route and heat treated at different temperatures showed an exponential increase in the particle size with temperature.

3.2. Mossbauer spectroscopic observations

Fig. 3 shows Mössbauer spectrum of $CoFe_2O_4$ prepared by the DME route, a doublet with an isomer shift and quadruple splitting of 0.31 and 0.67 mm/s was observed due to superparamagnetic relaxations, indicating that the cobalt ferrite particles are single domain particles. Fig. 4(a and b) shows room temperature Mössbauer spectra of microcrystalline $CoFe_2O_4$ prepared by SS route under two different cooling condition from 1000 °C, (SS(RT) and SS(HT)). In spinel system like AB_2O_4 each metal ion in the octahedral site is surrounded by six tetrahedral sites as the second nearest neighbors connected by the oxygen anion. In a complete inverse spinel system all divalent ions are in octahedral site, but in a partial inverse spinel system like $CoFe_2O_4$, a fraction of cobalt ion enters into the second coordination sphere (tetrahedral site). Entering of cobalt ion in to tetrahedral site leads to change in the configuration of Fe (III) in octahedral site. Fe(III) ions in octahedral site can have different configuration with cobalt (II) and iron (III) in available six tetrahedral sites. This configuration leads to difference in the spin transfer from tetrahedral site to octahedral site via oxygen affecting hyperfine field of Fe(III) at octahedral site (super transferred hyperfine interaction) [18] manifesting in higher FWHM observed in the Mossbauer spectra for Fe(III) at octahedral site. Fitting of the Mössbauer spectra was carried out by considering the above phenomenon. Considering a random distribution of Fe(III) and Co(II) available on the six tetrahedral sites (6Fe:0Co, 5Fe:1Co, etc.,), the Fe(III) ion in the octahedral sites can have different configuration given by Eq. (1) [19]. Intensity of each sub-spectra of octahedral site is given by the probability function $P(c, n)$:

$$P(c,n) = \frac{6!}{n!(6-n)!}(1-c)^{6-n}c^n \quad (1)$$

where c is the fractional occupation of the site in the bulk and n indicates the number of Co(II) on tetrahedral-site. Mössbauer fit parameter like isomer shift (IS), hyperfine magnetic field $\langle B \rangle$ and

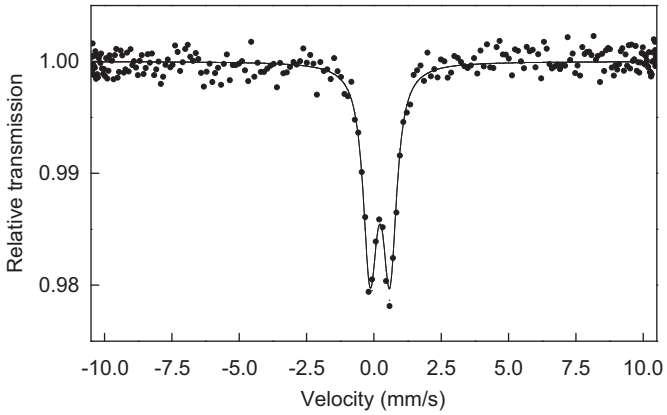

Fig. 3. Room temperature Mössbauer spectrum of $CoFe_2O_4$ prepared by DME route.

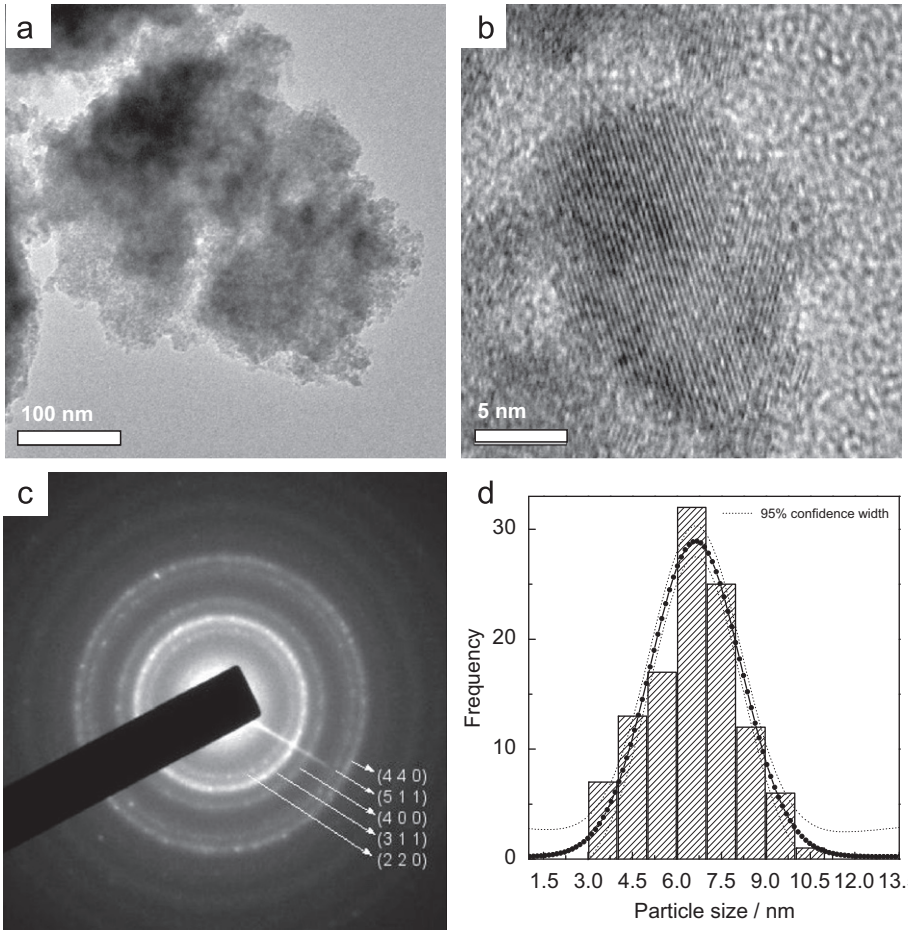

Fig. 2. (a) TEM micrographs of $CoFe_2O_4$ prepared by DME route, (b) high resolution TEM image, (c) SAED pattern and (d) particle size histogram.

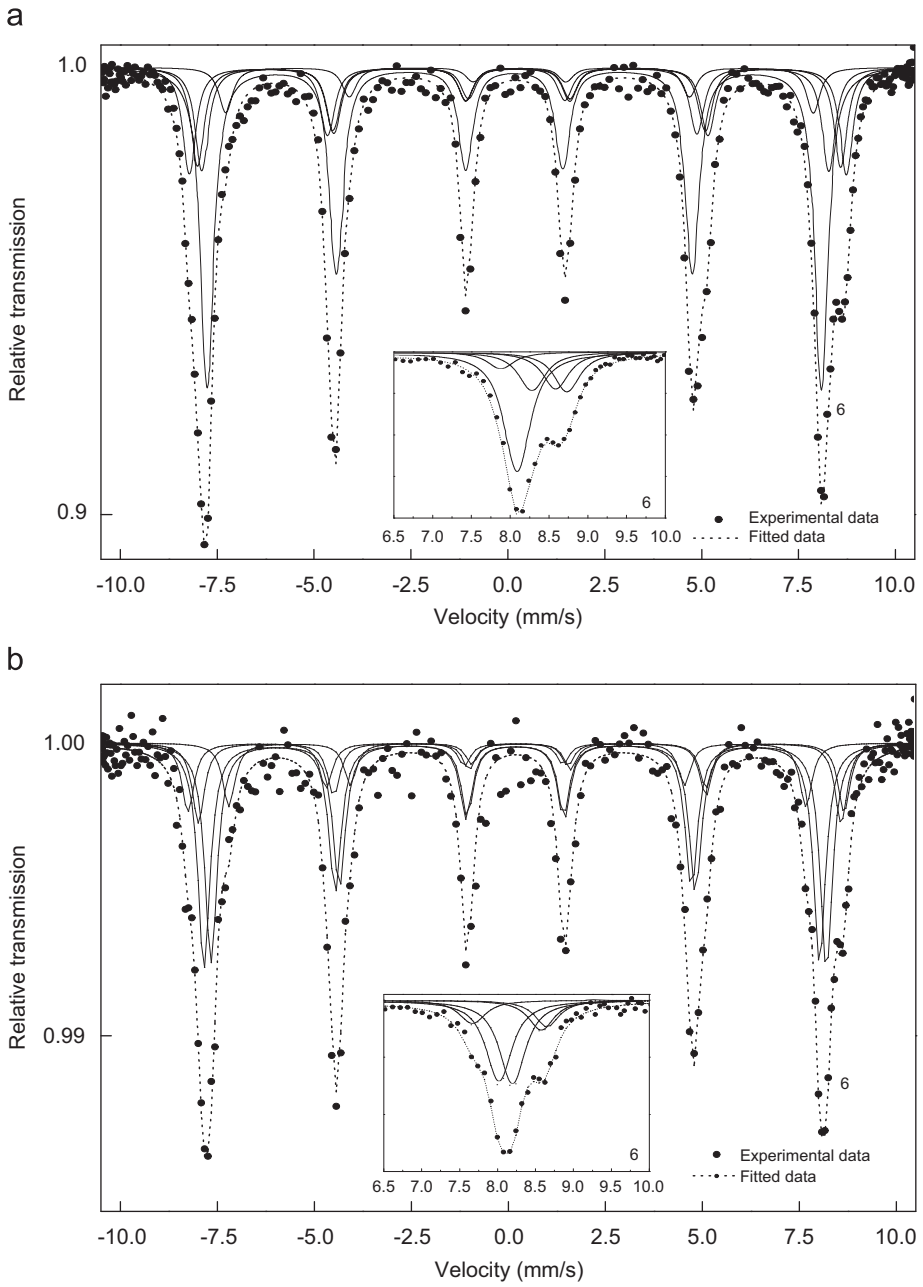

Fig. 4. Room temperature Mössbauer spectrum of $CoFe_2O_4$ [(a) SS(RT), (b) SS(HT_N)].

relative intensity I_{rel} of different configurations are listed in Tables 2 and 3. Isomer shift and hyperfine field values were used for assigning the Fe(III) in tetrahedral (A) and octahedral site (B_n), relative intensity of the each iron environment was used for calculating the cationic distribution in spinel. The $CoFe_2O_4$ SS(HT) which is high temperature frozen phase shows 69% of cobalt ions in B-site compared to 95% in SS(RT) sample which is low temperature phase. This computed cation distribution is in good agreement with the literature reports [19,20].

3.3. Raman spectroscopy observation

Micro-Raman spectroscopy is a powerful and sensitive tool for characterization of thin films and powders. This technique is useful in understanding the microstructure of the materials down to nano-size domain. Ferrites, MFe_2O_4 crystallizes in cubic structures belong to the space group $Fd\bar{3}m$ (O_h^7, No. 227). One complete unit cell contains 56 atoms ($Z=8$) and the smallest Bravais cell consists of only 14 atoms ($Z=2$). Factor group analysis predicts following phonon modes for the spinel structure, namely A_{1g} (R), E_g (R), T_{1g}, $3T_{2g}(R)$, $2A_{2u}$, $2E_u$, $4T_{1u}$ (IR) and $2T_{2u}$. Out of these phonon modes, five are Raman active, namely A_{1g}, E_g and $3T_{2g}$. Cation redistribution in the tetrahedral and octahedral sites alter the symmetry of the crystal structure into $I4_1/amd$ space group with more number of active vibrational modes in Raman spectrum. Factor group analysis showed 10 Raman phonon modes ($2A_{1g}+3B_{1g}+B_{2g}+4_{Eg}$) for such lowered symmetric system. Cation distribution and its effect on Raman spectrum of spinel have been extensively reviewed by Lazzeri et al. [21] and Wijs et al. [22], on $MgAl_2O_4$ spinel. Both the studies have demonstrated the usefulness of Raman data in interpreting the cation redistribution in spinel system. Fig. 5(a, b) shows the Raman spectra for room temperature (SS(RT)) and high temperature phase (SS(HT) of microcrystalline $CoFe_2O_4$. Both these

Table 2
Mössbauer fit parameter of $CoFe_2O_4$ under different cooling condition, (SS(RT) and SS(HT_N)).

Sample	Site	Isomer shift (mm/s)	Hyperfine field (T)	Intensity (%)	Cationic distribution
$CoFe_2O_4$ (SS(RT))	A	0.28	49.1	47.6	$[Fe_{0.95}Co_{0.05}](Co_{0.95}Fe_{1.05})O_4$
	B_0	0.37	52.6	15.7	
	B_1	0.39	51.4	14.6	
	B_2	0.30	50.2	15.3	
	B_3	0.40	47.0	6.8	
$CoFe_2O_4$ (SS(HT_N))	A	0.29	49.7	34.3	$[Fe_{0.69}Co_{0.31}](Co_{0.69}Fe_{1.31})O_4$
	B_0	0.31	52.4	10.4	
	B_1	0.40	51.3	12.2	
	B_2	0.29	48.6	33.4	
	B_3	0.34	46.1	9.7	

Table 3
Mössbauer fit parameter for $CoFe_2O_4$ prepared by DME route.

Sample	Isomer shift[a] (mm/s)	Quadruple splitting	FWHM
$CoFe_2O_4$ (DME)	0.31	−0.67	0.74

[a] Isomer shift reported against α-Fe).

samples showed six peak maxima at 210, 312, 470, 575, 624 and 695 cm^{-1}, respectively. Assignment of these phonon modes were carried out in accordance with the literature reports [23]. Frequencies above 600 cm^{-1}, i.e., peak maxima at 624 and 695 cm^{-1} are due to A_{1g} symmetry involving symmetric stretching of oxygen atom with respect to metal ion in tetrahedral void, tetrahedral breath mode (TBM). The other low frequency phonon modes are due to metal ion involved in octahedral void (BO_6), i.e., E_g and $T_{2g}(3)$. These modes correspond to the symmetric and antisymmetric bending of oxygen atom in M–O bond at octahedral voids [24].

Mössbauer spectroscopic analysis showed decrease in inversion parameter for the high temperature phase (SS(HT)) indicating redistribution of higher amounts of Co(II) ion into tetrahedral site at higher temperature. Raman spectrum of the high temperature phase and room temperature phase are identical with respect to the peak maxima and FWHM, but spectrum shows a marked difference in relative intensity between the phonon modes at 624 and 695 cm^{-1}, indicating effect of cation distribution on the Raman spectrum of the ferrite system. High temperature phase with higher inversion parameter shows relatively higher intensity of 624 cm^{-1} vibrational mode compared to room temperature phase. Relative intensity ratio between 695 and 624 cm^{-1} of phonon modes, I_ν for high temperature phase was 2.58 ($\pm$0.11) and low temperature phase was 3.88 ($\pm$0.29). $CoFe_2O_4$ prepared by different quenching rate, i.e., by liquid nitrogen, ice cooled water and ambient air condition showed no change in the Raman shift or intensity of the vibrational modes. Cation distribution in the three samples SS (HT_N), SS(HT_W) and SS(HT) are same. Phonon vibrational mode at 624 cm^{-1} may be related to cationic distribution or Co–O bond in tetrahedral site as a direct correlation between cobalt in tetrahedral site and vibrational mode at 624 cm^{-1} which is supported by the Mössbauer data.

3.3.1. *Effect of laser power variation on Raman spectrum of bulk $CoFe_2O_4$.*

Fig. 6 shows Raman spectra of $CoFe_2O_4$ (SS(RT)) recorded under different laser power from 0.5 to 25 mW. Laser power was varied to see the effect of surface temperature on the Raman spectra. Two

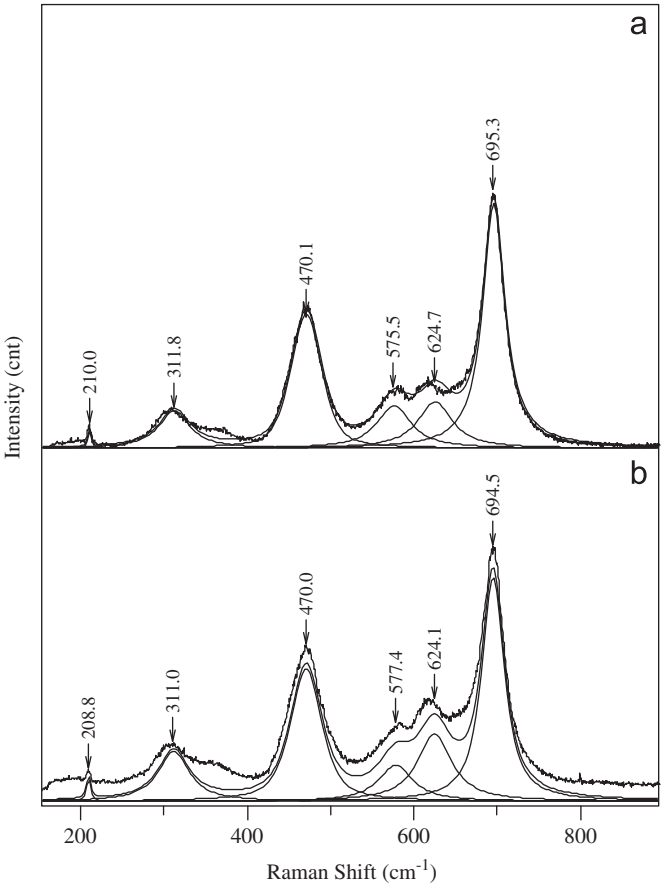

Fig. 5. Raman spectrum of $CoFe_2O_4$: (a) SS(RT) and (b) SS(HT_N).

major differences were observed. Red shift in the phonon mode and change in the relative intensity between the two vibration modes $A_{1g}(1)$ and $A_{1g}(2)$. Increase in laser power, led to increase in the surface temperature of the sample which has softened the vibrational modes of spinel lattice system. This softening resulted in the red shift of vibrational mode (0.02 cm^{-1}/K)[25]. Inset in Fig. 6 shows the variation in the strength of A_{1g} phonon mode with laser power; data shows a linear dependence on laser power with intercept or zero power laser vibrational mode for $A_{1g}(1)$ mode is 694.84 cm^{-1}. $CoFe_2O_4$, which is sensitive to the cation redistribution with respect to temperature showed change in relative intensity of phonon modes of $A_{1g}(1)$ and $A_{1g}(2)$ with the increase in laser power. Relative intensity ratio, I_ν with laser power showed an exponential decrease with pre-exponentional factor of 3.82 and a decay coefficient of 15.53/mW, which is proportional to surface temperature (Fig. 7).

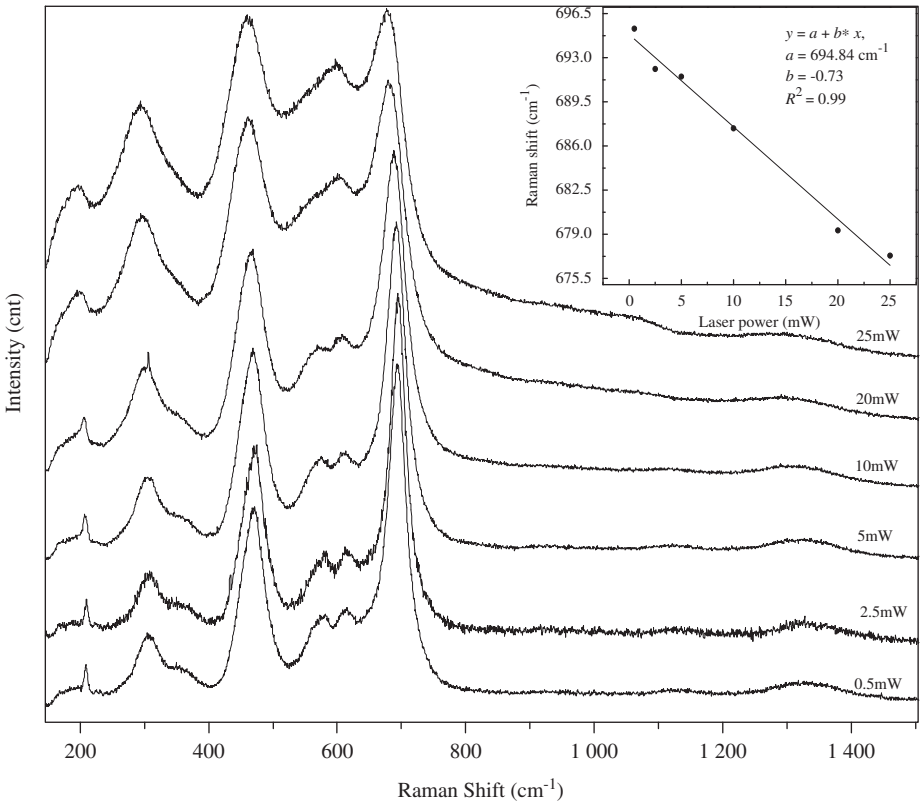

Fig. 6. Raman spectrum of $CoFe_2O_4$ (SS(RT)) recorded with different laser power.

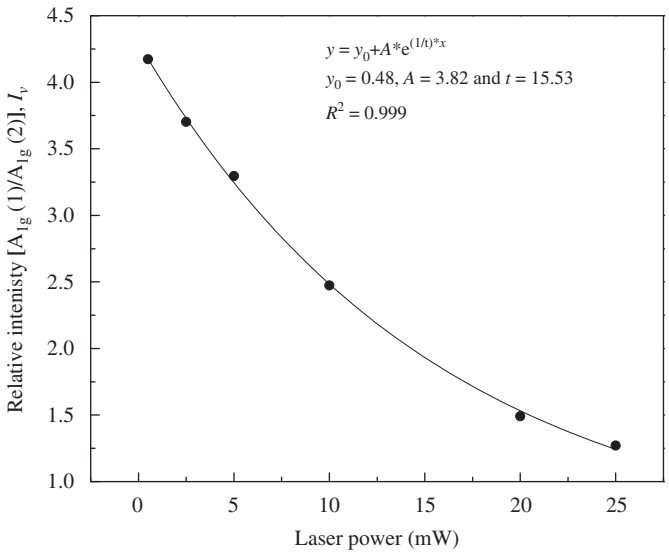

Fig. 7. Variation of I_v with laser power.

Raman spectrum was recorded on the $CoFe_2O_4$ using 0.5 mW laser power which has already experienced laser power varying from 0.5 to 25 mW. The spectra showed no change in the vibrational modes but change in the relative peak ratios of $A_{1g}(1)$–$A_{1g}(2)$. A value of 3.2 was seen as compared to ratio of 4.2 for Raman spectra (SS(RT)) taken before increasing the laser power. This observation indicates effect of laser power variation on the cation distribution in $CoFe_2O_4$ spinel system. Thus, these experimental observations clearly show the sensitiveness of cation distribution in ferrite systems towards the temperature (as affected by the laser power).

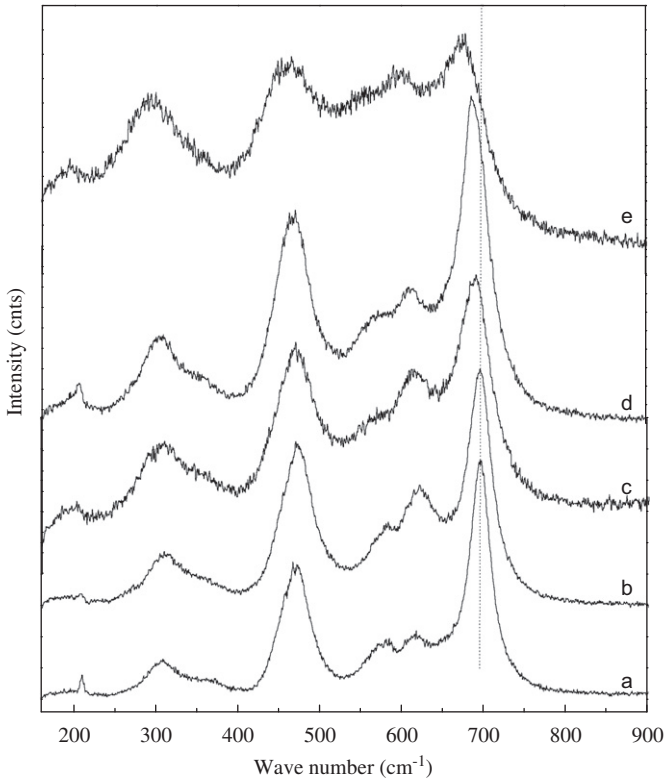

Fig. 8. Raman spectra different size $CoFe_2O_4$: (a) SS (RT), (b) PC route – 900 °C, (c) PC route – 700 °C, (d) PC route – 500 °C, (e) DME.

3.3.2. *Effect of particle size on Raman spectrum*

In crystalline materials, conservation of momentum vector '*q*' forces the first order Raman scattering phonon near to the center of

Table 4
Raman phonon modes of $CoFe_2O_4$ prepared by different routes.

Sample	Raman shift/FWHM (cm^{-1})					
	$A_{1g}(1)$	$A_{1g}(2)$	$T_{1g}(2)$	$T_{1g}(1)$	E_g	$T_{1g}(3)$
$CoFe_2O_4$ (SS(RT))	695.3 (31.7)	624.6 (50.0)	470.1 (43.7)	575.4 (50)	311.8 (45)	210.0 (5.3)
$CoFe_2O_4$ (PC -900)	692.8 (44.2)	620.8 (53.3)	469.6 (52.8	572.6 (59.3)	311.1 (65.5)	203.4 (10.0)
$CoFe_2O_4$ (PC-700	688.4 (43.9)	613.1 (50)	468.1 (52.5)	563.2 (45.0)	309.0 (69.5)	204.9 (10.0)
$CoFe_2O_4$ (PC-500)	685.6 (55.5)	614.8 (50.0)	470.7 (66.3)	560.8 (45.0)	310.3 (86.8)	197.3 (10)
$CoFe_2O_4$ (DME)	674.8 (65.4)	604.9 (66.9)	460.7 (100.0)	547.7 (75.0)	293.2 (89.0)	190.2 (75.0)

Brillouin zone ($q=0$) to contribute. Moreover, in small dimension systems such as nano-size crystals, due to lack of long range order, scattering with $q \neq 0$ is allowed leading to broadening and shift of peaks position in the Raman spectra. Fig. 8 shows Raman spectra of $CoFe_2O_4$ in different size domains. Vibrational modes and FWHMs for ferrite with different size domain are tabulated in Table 4. Raman spectra of $CoFe_2O_4$ prepared by DME route shows peak maxima at 674.8 and 604.9 cm^{-1} for $A_{1g}(1)$ and $A_{1g}(2)$ TBM phonon mode. A 20.5 cm^{-1} red shift with broadening of peak was seen for both modes compared to microcrystalline sample (SS route). Raman peak shift and broadening of A_{1g} peak can be explained by phonon confinement model described by Zi et al. [26,27]. Raman intensity in the μv polarization for backscattering configuration is given by

$$I_{\mu\nu}(\omega) \propto [n(\omega)+1]\sum_j \delta(\omega-\omega_j)\left|\Delta\alpha_{\mu\nu}(j)\right|^2 \quad (2)$$

where $[n(\omega)+1]$ is the Bose–Einstein population factor and $\Delta\alpha_{\mu\nu}(j)$ is the variation of polarization tensor due to the phonon mode ω_j. Raman shift due to the confinement can be described by this model using the relation

$$\Delta\omega = \omega(L)-\omega_0 = A\left(\frac{a}{L}\right)^{\gamma} \quad (3)$$

where $\omega(L)$ is the Raman shift with particle size L. ω_0 is the frequency at the Brillouin zone center and a is the lattice constant of the crystal. The fit parameters A and γ describes the vibrational confinement in nano-crystallites. Fit parameter γ describes the shape and size of the crystal. Fig. 9 shows variation of the Raman shift in $CoFe_2O_4$ with particle size, with a best fit of $A=104.5$ cm^{-1} and $\gamma=0.8$ reflecting the phonon confinement in the $CoFe_2O_4$. Thus, this relationship (Eq. (3)) with the above constants can be used for estimating size of the $CoFe_2O_4$ particles. Relative intensity ratio I_ν for phonon mode $A_{1g}(1)$ and $A_{1g}(2)$ with different size of ferrites prepared by PC route and DME route were compared to understand the cation distribution with particle size. I_ν for the ferrite particle in single domain region (DME route) shows a value of 1.1 and PC route with particle size less than 125 nm showed a value of 2.34 ($\pm$ 0.50). Relative peak intensity ratio I_ν for different size of ferrite particles shows the cation redistribution taking place with particle size and distribution is tending towards normal spinel configuration compared to bulk which is 95% inverse spinel configuration, i.e., 5% of cobalt ions are in tetrahedral void.

4. Conclusion

$CoFe_2O_4$ was synthesized through different route to get particle size domains ranging from 6 to 500 nm (bulk). XRD and TEM data confirmed the spinel phase and size domain, respectively. The cation distribution in the spinel was followed using Mössbauer and Raman spectroscopy. Microcrystalline ferrite prepared with different cooling condition showed difference in the cation distribution, ferrite with controlled cooling condition stabilized cation distribution with inversion parameter of 0.95 and quenched sample with an inversion parameter of 0.69. Cation redistribution taking place at high temperature phase could be ascertained using Raman spectroscopy. Relative intensity I_ν between the two vibrational mode at 695 and 624 cm^{-1} decreased with the decrease in the inversion parameter of $CoFe_2O_4$. Increase in the laser power for acquisition of Raman spectra showed change in the cationic distribution of the ferrite. With laser power or surface temperature increase cation distribution is stabilizing more towards normal configuration. Variation of Raman shift with particle size was compared and it followed the bond polarization model equation with $A=104$ cm^{-1} and $\gamma=0.8$ as constants. Vibrational mode of $A_{1g}(1)$ and $A_{1g}(2)$ in the Raman spectra with different size of particles clearly shows cation redistribution taking place with particle size. Thus occurrence of cation distribution in spinels and its dependence on size and temperature was proved conclusively.

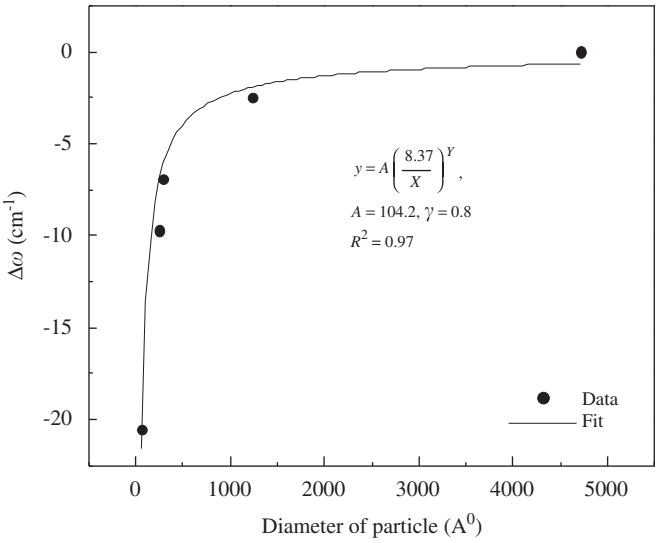

Fig. 9. Raman shift ($\Delta\omega$) against the diameter of the ferrite particle supported by confinement model.

References

[1] H.S.C. O'Neill, A. Navrotsky, American Mineralogist 68 (1–2) (1983) 181–194.
[2] Z.J. Zhang, Z.L. Wang, B. Chakoumaks, J.S. Yin, Journal of American Chemical Society 120 (1998) 4.
[3] T. Yu, Z.X. Shen, Y. Shi, J. Ding, Journal of Physics: Condensed Matter 37 (2002) L613.
[4] S.J. Figueroa, S.J. Stewart, Journal of Synchrotron Radiation 16 (Pt 1) (2009) 63–68.
[5] V. Sepelak, D. Baabe, D. Mienert, F.J. Litterst, K.D. Becker, Scripta Materialia 48 (2003) 5.
[6] F.S. Li, L. Wanga, J.B. Wang, Q.G. Zhou, X.Z. Zhou, H.P. Kunkel, G. Williams, Journal of Magnetism and Magnetic Materials 268 (3) (2004) 332–339.
[7] C.N. Chinnasamy, A. Narayanasamy, N. Ponpandian, K. Chattopadhyay, Materials Science and Engineering A 304–306 (2001) 983–987.
[8] S.K. Pradhan, S. Bid, M. Gateshki, V. Petkov, Materials Chemistry and Physics 93 (1) (2005) 224–230.

[9] W.S. Chiu, S. Radiman, R. Abd-Shukor, M.H. Abdullah, P.S. Khiew, Journal of Alloys and Compounds 459 (1-2) (2008) 291–297.
[10] J.A. Sawicki, H.A. Allsop, Journal of Nuclear Materials 240 (1) (1996) 22–26.
[11] A.-H. Lu, E.L. Salabas, F. Schüth, Angewandte Chemie International Edition 46 (8) (2007) 1222–1244.
[12] L.M. Fraas, J.E. Moore, J.B. Salzberg, The Journal of Chemical Physics 58 (9) (1973) 3585–3592.
[13] Z. Cvejic, S. Rakic, A. Kremenovic, B. Antic, C. Jovalekic, P. Colomban, Solid State Sciences 8 (8) (2006) 908–915.
[14] Z. Wang, Physical Review B 68 (9) (2003) 094101.
[15] P. Barpanda, S.K. Behera, P.K. Gupta, S.K. Pratihar, S. Bhattacharya, Journal of the European Ceramic Society 26 (13) (2005) 2603–2609.
[16] M.A. Laguna-Bercero, et al., Journal of Physics: Condensed Matter 19 (18) (2007) 186217.
[17] M.P. Pileni, Supramolecular Science 5 (1998) 321–329.
[18] F. van der Woude, G.A. Sawatzky, Physical Review B 4 (9) (1971) 3159.
[19] G.A. Sawatzky, F. Van Der Woude, A.H. Morrish, Physical Review 187 (2) (1969) 747.
[20] G.A. Sawatzky, F. Van Der Woude, A.H. Morrish, Journal of Applied Physics 39 (2) (1968) 1204–1205.
[21] M. Lazzeri, P. Thibaudeau, Physical Review B 74 (14) (2006) 140301.
[22] G.A. de Wijs, C.M. Fang, G. Kresse, G. de With, Physical Review B 65 (9) (2002) 094305.
[23] P.R. Graves, C. Johnston, J.J. Campaniello, Materials Research Bulletin 23 (11) (1988) 1651–1660.
[24] Z. Wang, P. Lazor, S.K. Saxena, H.S.C. O'Neill, Materials Research Bulletin 37 (9) (2002) 1589–1602.
[25] O.N. Shebanova, P. Lazor, Journal of Solid State Chemistry 174 (2) (2003) 424–430.
[26] J. Zi, H. Buscher, C. Falter, W. Ludwig, K. Zhang, X. Xie, Applied Physics Letters 69 (2) (1996) 200–202.
[27] Zi Jian, Physical Review B 55 (15) (1997) 9263.